Mechanomutable carbon nanotube arrays

Steven Cranford and Markus J. Buehler*

Center for Materials Science and Engineering and Laboratory for
Atomistic and Molecular Mechanics,
Department of Civil and Environmental Engineering,
Massachusetts Institute of Technology,
77 Massachusetts Ave., Room 1-235A&B,
Cambridge, MA 02139-4307, USA
E-mail: cranford@mit.edu
E-mail: mbuehler@mit.edu
*Corresponding author

Abstract: Here we present atomistic-based multi-scale simulation studies of a magnetically active array of carbon nanotubes to illustrate the concept of mechanomutability. We show that applying external fields, it is possible to change the nanostructure and to induce a desired mechanical response. Direct numerical simulations are reported that illustrate this concept via mechanical testing through nanoindentation. Specifically, the contact stiffness of an array of carbon nanotubes can be changed reversibly from approximately 73 MPa to 910 MPa due to the application of an external field. A hierarchical approach (coarse grain molecular modeling) is implemented to develop a framework that can successfully collaborate atomistic theory and simulations with material synthesis and physical experimentation, and facilitate the progress of novel mechanomutable structural materials.

Keywords: mechanomutability; nanomechanics; deformation; multi-scale modeling.

Biographical notes: Steven Cranford is a PhD student in the Department of Civil and Environmental Engineering, Massachusetts Institute of Technology, Cambridge, MA 02139 USA.

Markus J. Buehler currently holds the Esther and Harold E. Edgerton Career Development Professorship, Department of Civil and Environmental Engineering, Massachusetts Institute of Technology, Cambridge, MA 02139 USA.

1 Introduction

Carbon nanotubes (CNTs) constitute a prominent example of structural nanomaterials, with many potential applications that could take advantage of their unique mechanical properties. Synthesis techniques have become adept at producing arrays or carbon

nanotube forests consisting thousands of aligned nanotubes with similar diameters, lengths and aspect ratios (Qi et al., 2003). The properties of such nanotube arrays can be exploited to produce novel mechanomutable materials with unique, amplified, and controlled mechanical properties.

1.1   Discussion of mechanomutable materials

Advances in material modeling and simulation at the nanoscale combined with new techniques in material fabrication give rise to a new paradigm of material design. Multi-scale theoretical approaches can lead to the bottom-up design of purpose-specific materials from the atomistic to the continuum levels. As a direct result, a new class of mechanomutable heteronanomaterials is being investigated. Such a material is defined as possessing spatially localised and controlled nanoscale units of varying components that change the mechanical properties reversibly in response to external stimuli. Mechanomutable materials differentiate themselves from simple responsive materials in the sense that mechanical properties do not react to external phenomena in an ad hoc manner based on chemical behaviour, but can be controlled via tunable stimuli with *designed intent*.

The keystone to the development of mechanomutable materials is a fluid and synergistic multiscale theoretical foundation from atomistic scales to the mesoscale to macroscale continuum-level constitutive modeling. Hierarchical 'handshaking' at each scale is crucial to predict structure-mechanical property relationships, to provide fundamental mechanistic understanding of mechanomutable behaviour, and to enable predictive material design optimisation to guide synthetic design efforts.

The use of heteronanostructures provides many exciting possibilities for mechanomutable materials design that have not yet been realised; in particular high spatial resolution interactions with nanoscale objects and unique and amplified mechanical robustness (Buehler, 2006a; Tai et al., 2007; Tai et al., 2006). Such materials can be introduced as unique structural components in a global system as a means to control robustness or as high-throughput, high spatial sensitivity tunable sensor (Ruan et al., 2003).

1.2   Mechanomutable carbon nanotube arrays

A candidate for mechanomutability is magnetically active nanotube composites. This paper will describe the preliminary investigations of a magnetically active array of carbon nanotubes to illustrate the concept of mechanomutability. Initial investigations are concentrating on carbon nanotube array due to an extensive theoretical background on molecular modeling and physical synthesis. A current and vast knowledge base of CNT behaviour provides promising candidate for development of mutable nanotube composites, as interactions of CNTs at nano-scale can be shown to result in unique, amplified, and reversible meso-/macroscale mechanical properties. Carbon nanotubes provide a straightforward template to illustrate the benefits of a hierarchical molecular dynamic approach (atomistic to mesoscale), as well as the simulation of experimental techniques that probe mechanical properties (i.e., nanoindentation). A fundamental understanding of the properties of individual CNTs, assemblies of CNTs in bundles (Zhang et al., 2005), or CNTs in conjunction with biological molecules such as DNA

(Gao et al., 2003) may enable new technologies and to engineer CNT based mechanomutable devices.

1.3 Outline of this paper

The plan of this paper is as follows. In Section 2, the computation method to construct the mesoscopic nanotube array model will be described (Section 2.1). A series of full atomistic calculations to determine fundamental mechanical parameters for individual carbon nanotubes will be discussed. The mesoscale model is formulated, followed by a description of the model itself (Section 2.2). Section 2.3 discusses the application of a magnetic field to nanotube array, while Section 2.4 will discuss a molecular dynamic nanoindentation simulation technique. In Section 3, the results of nanoindentation simulations will be presented, as well as preliminary material property calculations. The results and implications of this model are discussed in Section 4.

2 Computational methods

In the following sections, we describe our atomistic based multi-scale simulation approach used to develop a mesoscale description of carbon nanotube arrays. It is challenging to model CNT arrays using classical macroscopic techniques due to the interactions between individual nanotubes at the nanoscale where weak dispersive van der Waal interactions (vdW) play a prominent role in the governing mechanics. As such, a multi-scale technique is required to accurately capture the behaviour of CNT arrays. Full atomistic models have proven to be a quite useful approach in understanding the mechanical behaviour of CNTs (Guo et al., 2006; Lu and Zhang, 2006; Yeak et al., 2005; Lu and Bhattacharya, 2005; Pugno and Ruoff, 2004; Marques et al., 2004; Zhou and Shi, 2002). However, such models are limited to very short time- and length-scales so that a direct comparison with experimental scales is difficult. To overcome these limitations, a mesoscale model representing CNTs as a collection of beads connected by spring-like molecular multi-body interatomic potentials is implemented. Such bead-type models have been implemented for several other molecular systems and applications (Molinero and Goddard, 2005; Lamm et al., 2003; Underhill and Doyle, 2004; Maiti et al., 2005). The mesoscale model is capable of treating the deformation physics of large assemblies of carbon nanotubes while maintaining the key atomistic properties.

2.1 'Finer-trains-coarser' approach

A 'finer-trains-coarser' approach is implemented to produce a mesoscale model derived solely from atomistic calculations. A series of full atomistic calculations of mechanical test cases (test suite) is implemented to derive a set of parameters that describe the molecular-scale or meso-scale behaviour.
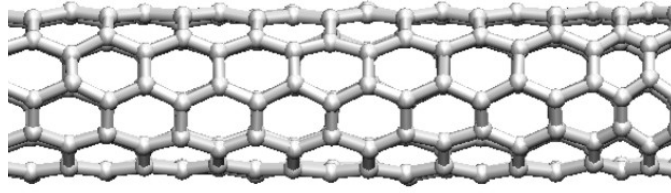
2.1.1 Atomistic calculations (fine)

The test suite consists of the following three loading cases:

1   tensile loading to determine Young's modulus as well as fracture stress and strain

2   bending to determine the bending stiffness of CNTs

3   an assembly of two CNTs to determine the adhesion energy.

All studies were carried out using (5,5) armchair single wall CNTs (SWCNTs) through classical molecular dynamics. For a more detailed description of the atomistic simulations and results, the reader is referred to Buehler (2006b). Here, we provide only a brief review of the multi-scale approach. Figure 1 depicts the molecular model of the nanotube.

Figure 1   Schematic representation of CNT atomistic model

Tensile deformation of a CNT is modeled by keeping one end of the CNT fixed while slowly displacing the other end in the axial direction of the tube. The virial stress tensor component in the loading direction is used to extract the stress, σ, as a function of applied uniaxial strain, ε. The stress-strain relationship can then be used to determine Young's modulus

$$E = \frac{\partial \sigma}{\partial \varepsilon} \approx \frac{\Delta \sigma}{\Delta \varepsilon} \tag{1}$$

The loading case is shown in Figure 2(a). At large strains, defects were formed that lead to the fracture of the carbon nanotube. As such, the fracture strain (ε_F) can be directly taken from the tensile loading results. Figure 3 contains result of calculations carried out with three different displacement-loading rates.

Figure 2   Mechanical loading cases for atomistic simulation (see online version for colours)
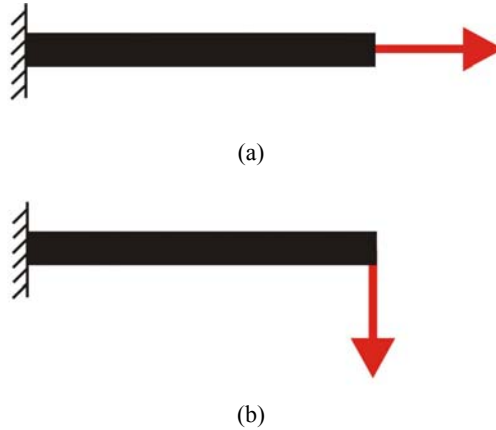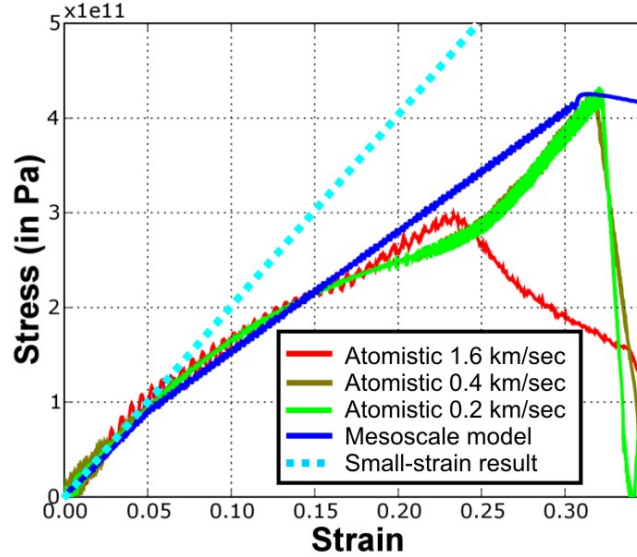

(a)

(b)

Figure 3 Stress-strain results for atomistic and mesoscopic tensile loading (see online version for colours)

Similar to the tensile test, a simple computational experiment is implemented to describe the bending of a CNT by clamping it at the outermost left boundary and applying a force at the right end of the CNT, as shown in Figure 2(b). By measuring the bending displacement d, the bending stiffness EI is then given by

$$EI = \frac{FL^3}{3d},\qquad(2)$$

where F is the applied bending force, and L is the total length of the cantilevered segment, as depicted in Figure 2(b).

Due to the ultimate interest in modeling an array of CNTs, the interaction between adjacent nanotubes was also simulated. Primary interaction forces are weak dispersive interactions, such as van der Waal's forces. It is assumed that no covalent bonds may form between different CNTs. The simulation results in the equilibrium distance between CNTs as well as the adhesion energy between two CNTs. Further, the molecular dynamics simulation results suggest that pair-wise interaction between different CNTs represents a reasonable model.
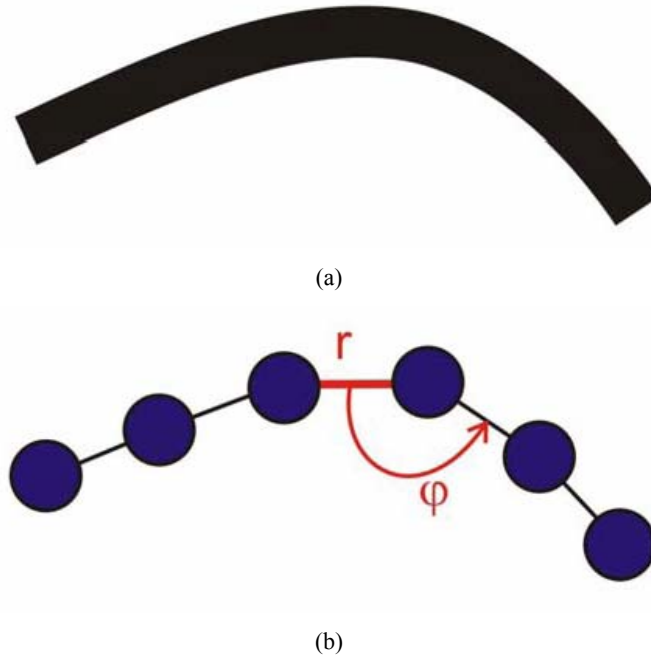
2.1.2 Mesoscopic parameter derivation (coarse)

Next the method in deriving parameters for a mesoscale bead-type model of CNTs from the full atomistic calculation results is discussed. A schematic illustration is presented in Figure 4. The mesoscale model is represented by a function of the total energy of the system expressed as

$$E_{System} = E_T + E_B + E_{weak} \tag{3}$$

where E_T is the energy stored in the chemical bonds due to axial stretching, E_B is the energy due to bending, and E_{weak} is the energy due to weak interactions. The total energy contribution of each is calculated by a sum over all pair-wise (distance) and triple (angular) interactions in the system.

Figure 4   (a) Atomistic and corresponding (b) mesoscopic model of a CNT (see online version for colours)

(a)

(b)

For axial stretching, a simple harmonic spring is used to determine the energy between all pairs of particles in the system, given by

$$E_T = \sum_{pairs} \phi_T(r) \tag{4}$$

$$\phi_T(r) = \frac{1}{2} k_T \left(r - r_0\right)^2, \tag{5}$$

with k_T as the spring constant relating distance, r, between two particles. For bending, the bending energy is given by a sum over all triples in the system, given by

$$E_B = \sum_{angles} \phi_B(\phi), \tag{6}$$

$$\phi_B(\varphi) = \frac{1}{2} k_B \left(\varphi - \varphi_0\right)^2, \tag{7}$$

with k_B as the spring constant relating bending angle, φ, between three particles. Weak interactions (vdW) are defined by a Leonard-Jones 12:6 function, given by

$$E_{weak} = \sum_{pairs} \phi_{weak}(r),$$ (8)

$$\phi_{weak}(r) = 4\varepsilon\left(\left[\frac{\sigma}{r}\right]^{12} - \left[\frac{\sigma}{r}\right]^{6}\right)$$ (9)

with σ as the distance parameter and ε describing the energy well depth at equilibrium. In addition, the fracture properties can be introduced to the system via a bilinear model for axial stretching, or

$$\phi_T(r) = H\left(r_{break} - r\right)\begin{cases} \dfrac{1}{2}k_T^{(0)}(r-r_0)^2 & \text{if } r < r_1, \\[2mm] \dfrac{1}{2}k_T^{(1)}(r-r_1)^2 & \text{if } r \geq r_1. \end{cases}$$ (10)

Introducing the Heaviside function $H(a)$, which is defined to be zero for $a < 0$, and one for $a \geq 0$, and $k_T^{(0)}$ as well as $k_T^{(1)}$ for the small and large-deformation spring constants. Thus, the mesoscopic model can be defined by nine parameters: $k_T^{(0)}$; $k_T^{(1)}$; r_0; r_1; r_{break}; k_B; φ_0; σ, and; ε.

The results from the atomistic simulations are used to determine the nine parameters. The equilibrium distance, r_0, is user-defined, and equivalent to the bead spacing in the mesoscale model. The distance for the transition from small to large deformation, r_1, is taken by fitting the bilinear model to the stress-strain response. The distance at fracture, r_{break}, is simply taken as the distance at fracture strain. To develop the atomic interactions, we fit the force-stretch response to the stress-strain response obtained via atomistic calculations via the spring constant $k_T^{(0)}$ for small deformation. For large deformation, the parameter $k_T^{(1)}$ is determined by fitting the mesoscopic stress-strain results to the MD stress-strain curve.

Through energy conservation between the atomistic and the mesoscale model, we arrive at an expression for the bending stiffness parameter k_B. Further, the equilibrium angle, φ_0, is simply taken as 180 degrees (i.e. linear nanotubes). The LJ parameters, σ and ε, are chosen to reproduce the adhesion energy determined from full atomistic simulations. For a more detailed description of the parameter derivations, the reader is again referred to Buehler (2006b).

Thus, all parameters are defined solely from atomistic results. Table 1 gives numerical values for the mesoscopic model.

The 'finer-trains-coarser' approach eliminates the reliance on empirical tuning. From atomistic simulations using scales of femtoseconds and Angstroms a set of mesoscopic parameters was derived. The resulting mesoscale model enables modeling of the dynamics of systems with hundreds of ultra long CNTs over time scales approaching microseconds, facilitating a bridge between atomistic theory and simulation of actual physical experiments.

Table 1   Summary of mesoscopic parameters derived from atomistic modelling

Parameter	Units	Value
Equilibrium bead distance r_0	Å	10.00
Tensile stiffness, $k_T^{(0)}$	kcal/mol/Å^2	1000.00
Tensile stiffness, $k_T^{(1)}$	kcal/mol/Å^2	700.00
Hyperelastic parameter, r_1	Å	10.50
Fracture parameter, r_{break}	Å	13.20
Equilibrium angle, φ_0	degrees	180.00
Bending stiffness, k_b	kcal/mol/Å^2	14300.00
Dispersive parameter, ε	kcal/mol	15.10
Dispersive parameter, σ	Å	9.35

2.2   Simulation geometry and setup

The mesoscale model was created using grid of single bead-spring nanotube representations assembled to a vertically aligned array. An individual nanotube bead model consisted of 30 beads at 10 Å (300 Å total length). Atom pairs (representing bonds) and atom triples (representing angles) were also specified. The harmonic potential parameters for bonds and angles, Leonard-Jones 12:6 parameters were also input into the model. The result was 30 × 30 array of nanotubes (900 tubes total) spaced regularly at 20 Å. The first three atoms of each nanotube were fixed in all directions, representing a rigid substrate base. The model represents an array of nanotubes in a vacuum, corresponding to the environment conditions of the full atomistic calculations. Figure 5 depicts the initial geometry of the bead-spring model.

Upon running the model, random velocities are assigned to each bead, injecting kinetic energy into the system to attain an initial desired input temperature (300 K). The simulation implements a microcanonical (NVE) ensemble for energy conservation. The initial model was then run to obtain equilibrium conditions. Using a timestep of 30 femtoseconds, the model was simulated for approximately 30,000 timesteps (a timescale of approximately one nanosecond). This results in bundle formation due to weak interactions (van der Waals forces), which is reflective of actual CNT arrays. Figure 6 depicts the bundles at equilibrium.

The model was implemented using the massively paralysed modeling code LAMMPS (Plimpton, 1995) (http://lammps.sandia.gov/), capable of running on large computing clusters. The current investigations reported were carried out on single CPU Linux workstations. The LAMMPS code was extended to enable the treatment of the molecular interactions discussed in Section 2.1.2.

Figure 5 Mesoscale Bead-Spring model of CNT array (see online version for colours)
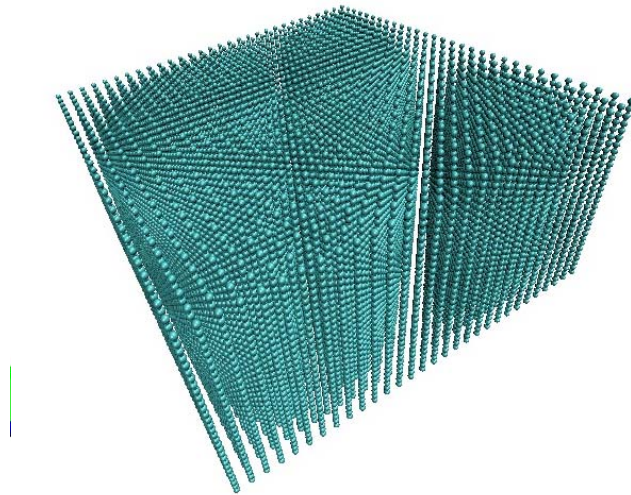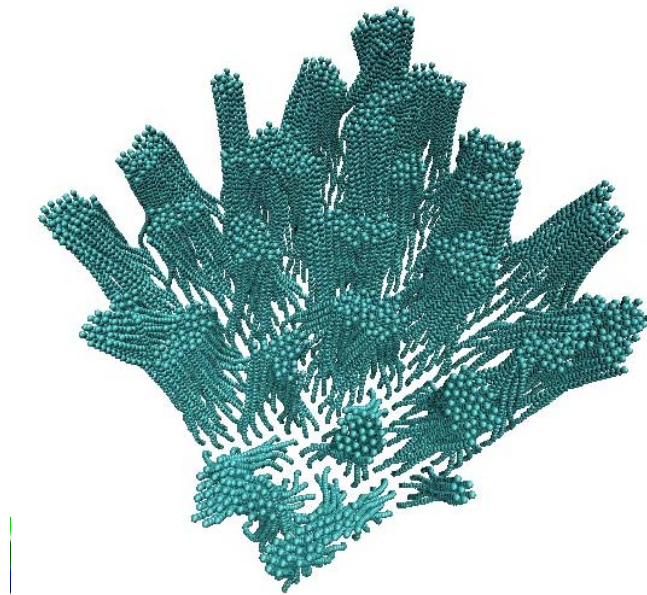

Figure 6 Formation of nanotube bundles at equilibrium (see online version for colours)

2.3   *Simulation of magnetic field*

What differentiates the current simulation of a CNT array is the investigation of the array under an external magnetic field to illustrate the ideology behind mechanomutability. The array is assumed magnetically active by the embedding/binding of magnetically active particles along the carbon nanotube during fabrication. Although the actual embedding of such particles has not been realised, concurrent studies are investigating the potential for poly(allylamine hydrochloride) (PAH) and poly(acrylic acid) (PAA) polyelectrolyte multiplayer (PEM) nanotube composites to be embedded with magnetite (Fe_3O_4) nanoparticles (Shiratori and Rubner, 2000). It is behooving to mention the intention of the current investigation is to provide the framework for the investigation of such magnetically active nanotube arrays, with CNTs providing one of many potential candidates as elementary constituents.

The magnetic field is simulated by applying a magnetic force via imposing an additional acceleration on each particle in the group. The force field can be thought of as a discrete body force in the sense the force per mass applied is resolved as a point force per atom. For the current simulation, each atom has equal mass, and thus the magnetic force is constant throughout the model. The force field itself is parameterised by a simple force magnitude (in units of force/mass) and directional vector. Table 2 depicts the parameters used for the current investigation.

Table 2   Summary of parameters for magnetic field

Parameter	Units	Value
Force magnitude	kcal- Å/grams	0.0006
Vector	n/a	(1,0,0) for axial field
		(0,1,0) for lateral field

Figure 7   CNT array under axial magnetic field, (a) top view and (b) side view (see online version for colours)

(a)   (b)
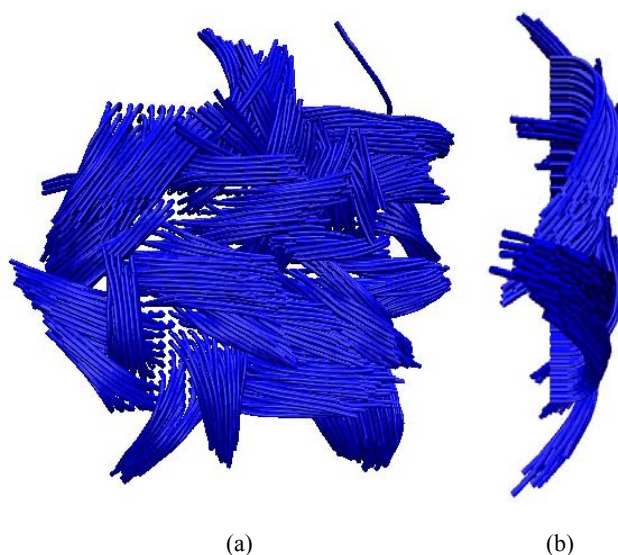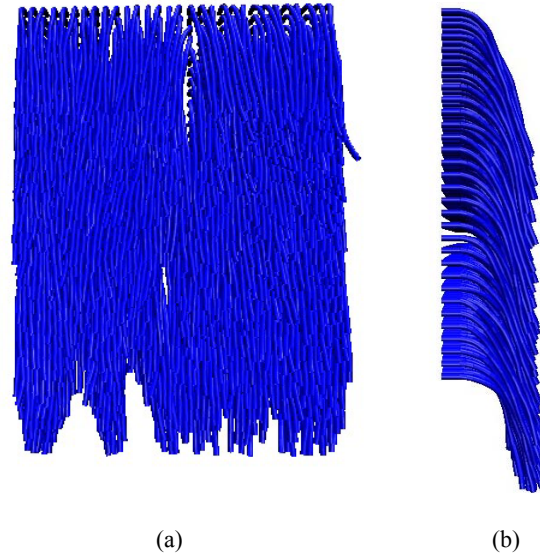
Figure 8 CNT array under lateral magnetic field, (a) top view and (b) side view (see online version for colours)

(a)   (b)

The variable magnetic force can be applied laterally or axially (with respect to nanotube orientation), cyclically or constant, etc. to investigate spatial orientation effects on mechanical properties as well as the responsive micro-pattern as function of array geometry and embedded magnetic particles. In addition to the affect on mechanical properties, the behaviour of such nanotubes under magnetic fields results in prospective magnetically actuated tunable nanostructures (Evans et al., 2007). Figures 7 and 8 depict the array model under magnetic fields.

2.4   Simulation of nanoindentation

Nanoindentation tests are currently one of the most commonly applied means of physically testing the mechanical properties of small volumes of materials. Such tests can result in the direct determination of parameters such as material hardness and modulus of elasticity, as well as provide a means to investigate material behaviour such as stress-strain relationships, the effect of strain-rate and robustness. The indentation process itself is simple: an indentor tip is pressed into the material, the force-penetration relationship is recorded, and then, after some time, the load is removed. The simulation of a nanoindentation at the mesoscale level is beneficial for a multitude of reasons. Primarily, such investigations can be linked to actual physical experiments, providing a critical connection between empirical results and theoretical basis. Further, nanoindentation results provide parameters applicable to the development of continuum-level formulations (i.e. elasticity models). As well, the simulation technique can be used as parametric study to investigate the behaviour of a material efficiently prior to physical empirical verification.

The mesocopic simulation of nanoindentation does not require the presence of a physical indentor (e.g. a collection of atoms/beads is not required). Indentation is simulated by the introduction an *indentor force field* within the simulation box, rather than an indentor itself. As such, the properties of the indentor need not be modelled, but rather only the affect of the indentor on the atoms. Simply put, the added indentor repels all atoms that touch it with a force, which can be adjusted by a simple parameter. For simplicity, a spherical indentor was used. The spherical indentor exerts a force of magnitude:

$$F(r_i) = -k(r_i - R)^2 , \tag{11}$$

where k is the specified force constant, r_i is the distance from the atom to the centre of the indentor, R is the radius of the indentor. The resulting force, $F(r_i)$ is repulsive and:

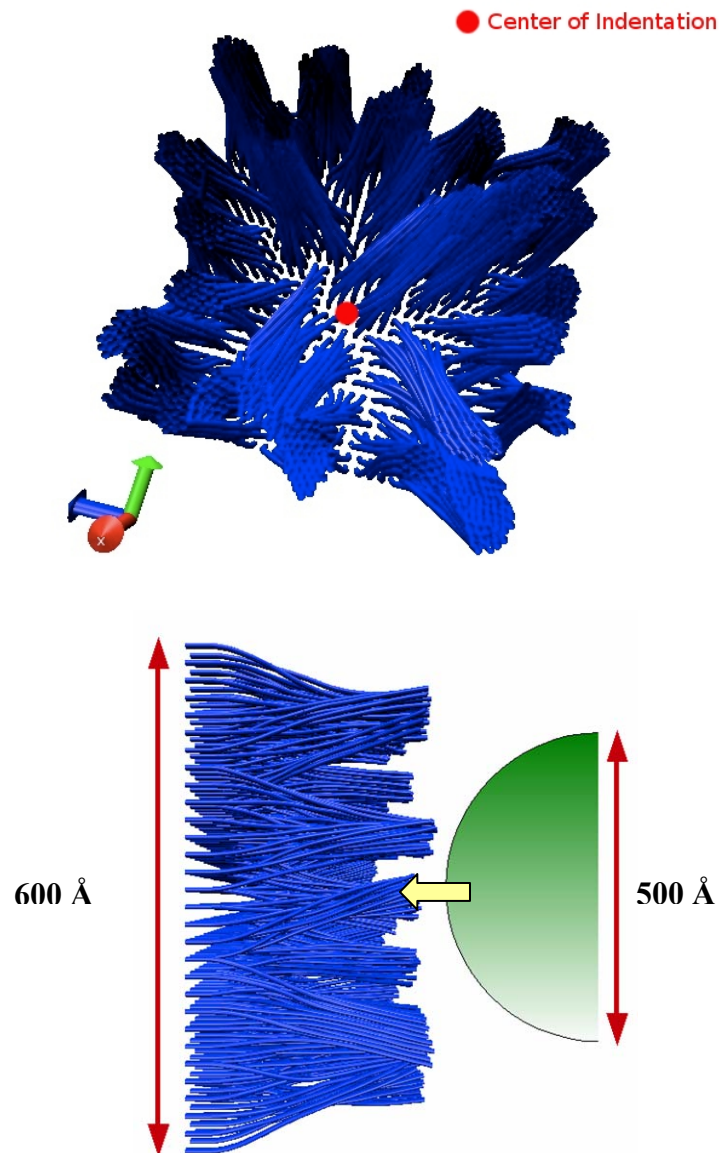$$F(r_i) = 0 \text{ for } r_i > R . \tag{12}$$

The velocity of the indentor is also specified, moving the centre of the spherical indentor during the simulation based on specified initial position. Both the force and position of the indentor tip are produced from the simulation, resulting the desired force-penetration relationship. Table 3 depicts the parameters used for the current investigation.

Table 3   Summary of parameters for nanoindentation

Parameter	Units	Value
k	(Kcal/mol- Å)/ $Å^2$	0.001
R	Å	250
Indenter velocity	Å/fs	0.000033

The mechanical properties of carbon nanotube arrays derived from nanoindentation are difficult to predict *a priori* due to interaction of bundles with the indenter. The resistance depends on a number of key structural features such as tube diameter, length, areal density, etc. As such, complex mathematical models have been developed to predict the mechanical properties of carbon nanotubes based on nanoindentation results (Qi et al., 2003). However, the current investigation concentrates on the mechanical properties of the nanotube array, not the individual nanotubes. Standard nanoindentation methods can be implemented to determine the relevant effective mechanical properties of the array and illustrate the mutable behaviour. Figure 9 shows the effect of the indenter on the CNT array, the location and direction of indentation, and the relative size of the indenter to the array.

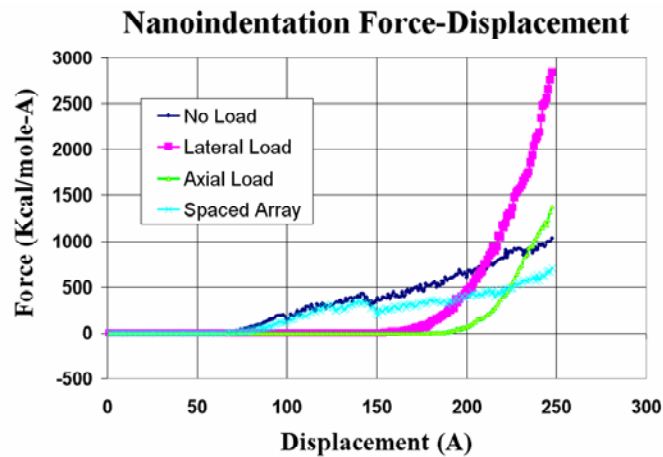**Figure 9** Nanoindentation CNT array (see online version for colours)
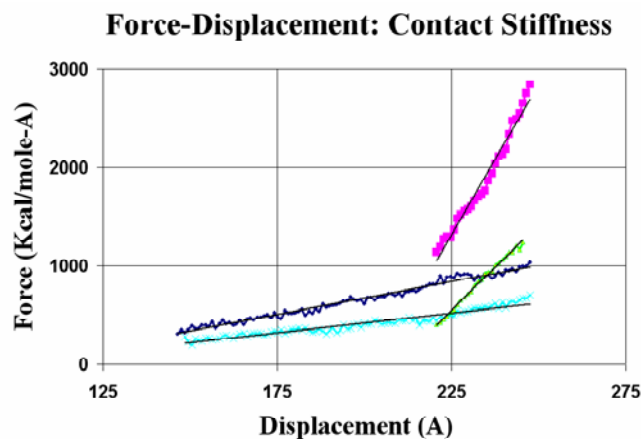
3   Computational results

Nanoindentation of the mesoscale model was simulated four times under different conditions to demonstrate the potential mechanomutability of the CNT array. First, the model was indented with no magnetic field present. Second, the model was indented with no magnetic field, but the density of CNTs decrease by 20% (attained by increasing the spacing in one direction to 25 Å). Third, an axial magnetic field was applied, followed by nanoindentation. Finally, a lateral magnetic field was applied, followed by nanoindentation. From each simulation, the force-penetration (*f-p*) information for the nanoindenter was extracted from the results. The results are shown in Figure 10(a).

The linear segment of the *f-p* curve is fitted to determine the contact stiffness of the indenter on the nanotube array. This linear fitting is shown in Figure 10(b). The numerical values of the contact stiffness are found in Table 4.

Figure 10   Force-penetration results for nanoindentation simulations (see online version for colours)

(a)

(b)

An analytical model for contact between a rigid indenter of defined shape can be used to model the contact stiffness (Sneddon, 1965; Pharr et al., 1992)

$$S = \frac{2\sqrt{A}}{\sqrt{\pi}} E_r,$$ (13)

where S is the contact stiffness and A is the contact area, and E_r is the reduced modulus. The contact area is calculated using the portion of the surface area of the spherical indentor at the maximum penetration depth, h_{max}, where

$$A = 2\pi R h_{max}.$$ (14)

The relationship assumes a homogenous isotropic elastic material, which is not the case for the current CNT array. However, more sophisticated methods of determining the contact stiffness of the CNT array are superfluous to the current investigation. The above relationship is deemed a suitable approximation.

Combining the CNT array and the indentor as a series of springs, the reduced modulus can also be represented by

$$\frac{1}{E_r} = \frac{1 - v_i^2}{E_i} + \frac{1 - v_{array}^2}{E_{array}}.$$ (15)

As the indentor is not modelled as a physical material, it is assumed that $E_i \gg E_{array}$. Further, the Poisson's ratio is small for an array of CNT (Hall, 2008) and deemed negligible. Thus, the above relationship is simplified to

$$\frac{1}{E_r} \approx \frac{1}{E_{array}}, \text{ or } E_r = E_{array}.$$ (16)

The results of the simulations are shown in Table 4.

Table 4 Summary of nanoindentation results

Simulation	Contact stiffness	Penetration depth	Contact area	Effective Young's modulus
	(kcal/mol/Å)	*(Å)*	*(nm²)*	*(MPa)*
No magnetic field	6.71	206	3235	72.6
No magnetic field (20% reduced density)	4.00	200	3141	44.0
Axial magnetic field	35.56	85	1337	599
Lateral magnetic field	61.46	110	1726	911

4 Discussion and conclusions

The coarse-grained model enables us to simulate experimental-scale phenomena using parameters derived from first-principles at the atomistic level. This approach allows the

investigation of global mechanical properties of a material caused by changes at the atomistic level – a fundamental goal of mechanomutability. The mesoscale model allows the representation of systems consisting of millions of atoms, but can simulate processes on the order of microseconds using the same developed techniques for molecular dynamics.

The current study depicts the mutable stiffness of an array of carbon nanotubes due to an imposed magnetic field. Although simplifications were implemented to determine the effective modulus of the nanotube array, the force-penetration relationships of the nanoindentation clearly depict changes in fundamental behaviour. The Young's modulus is dependent on the density of the carbon nanotubes (72.6 MPa for the first simulation compared to 44.0 MPa for the second, 20% less dense simulation – a decrease of approximately 40%), as well as their planar arrangement. The lateral magnetic force results in a regular pattern of nanotubes, resulting in the highest modulus (911 MPa). Imposing a magnetic field increased the effective modulus array surface eight (axial field) to 12 (lateral field) times – a significant mutable mechanical property. The calculated modulus of a single nanotube from atomistic calculations was approximately 2 TPa. Values for the current study ranging from 44.0 to 911 MPa is deemed reasonable for the relatively sparse array in a vacuum. It is also noted that the results of simulations one, three and four are all derived from the same geometry and are completely reversible (i.e. each modulus can be attained by varying the imposed magnetic field during the same simulation), thereby illustrating the mechanomutability of the system.

The mesoscale model inherently allows the efficient varying of array geometry (aspect ratios, array spacing, etc.) to investigate behaviour dependencies and pattern formation. Future investigations will determine if the modulus is uniquely tunable via magnetic stimuli, as well as the effects on surface and transport properties. The investigation also illustrates the ability to model physical experimental techniques (nanoindentation) to derive the physical properties, thus providing a crucial link between simulation and reality.

The coarse-graining technique of training a mesoscopic model based on atomistic results can be easily be implemented to investigate other systems and nanotubes, such as polymer and protein nanotubes, hybrid CNT-based materials, or the aforementioned poly(allylamine hydrochloride) (PAH) and poly(acrylic acid) (PAA) polyelectrolyte multiplayer (PEM) nanotube composites. The mesoscale modelling approach can also enable studies of nanotube arrays interacting with matrix materials, which is so far mainly addressed using experimental techniques (Barber et al., 2006). Such studies may ultimately prove the viability of mechanomutable hydrogel composites.

A key element of the modelling effort is the ability to form a closed loop between atomistic, micro- and mesoscale and the experimental analysis, enabling a full design approach. The successful simulation of nanoindentation at the mesoscopic level based solely on parameters derived from atomistic simulations illustrates this hierarchical approach coupled with a direct association to physical, experimental investigations.

Acknowledgements

Laboratory. Visualisation has been carried out using the VMD visualisation package (Humphrey et al., 1996).

References

Barber A.H., Cohen, S.R., Eitan, A., Schadler, L.S. and Wagner, H.D. (2006) 'Fracture transitions at a carbon-nanotube/polymer interface', *Advanced Materials*, Vol. 18, pp.83–87.

Buehler, M.J. (2006a) 'Cracking and adhesion at small scales: atomistic and continuum studies of flaw tolerant nanostructures', *Model. Sim. Mater. Science and Eng.*, Vol. 14, pp.799–816.

Buehler, M.J. (2006b) 'Mesoscale modeling of mechanics of carbon nanotubes: self-assembly, self-folding, and fracture', *J. Mater. Res.*, Vol. 21, No. 11, pp.2855–2869.

Evans B.A., Shields, A.R., Carroll, R.L., Washburn, S., Falvo, M.R. and Superfine R. (2007) 'Magnetically actuated nanorod arrays as biomimetic cilia', *Nano Letters*, Vol. 7, No. 5, pp.1428–1434.

Gao, H., Kong, Y., Cui, D. and Ozkan, C.S. (2003) 'Spontaneous insertion of DNA oligonucleotides into carbon nanotubes', *Nano Letters*, Vol. 3, pp.471–473.

Guo, X., Wang, J.B. and Zhang, H.W. (2006) 'Mechanical properties of single-walled carbon nanotubes based on higher order Cauchy-Born rule', *International Journal of Solids and Structures*, Vol. 43, pp.1276–1290.

Hall, L.J. (2008) 'Sign change of Poisson's ratio for carbon nanotube sheets', *Science* Vol. 320, pp.504–507.

Humphrey, W., Dalke, A. and Schulten, K. (1996) 'VMD: visual molecular dynamics', *Journal of Molecular Graphics*, Vol. 14, p.33.

Lamm, M.H., Chen, T. and Glotzer, S.C. (2003) 'Simulated assembly of nanostructured organic/inorganic networks', *Nano Letters*, Vol. 3, pp.989–994.

Lu, Q. and Bhattacharya, B. (2005) 'Effect of randomly occurring Stone-Wales defects on mechanical properties of carbon nanotubes using atomistic simulation', *Nanotechnology*, Vol. 16, pp.555–566.

Lu, H. and Zhang, L. (2006) 'Analysis of localized failure of single-wall carbon nanotubes', *Computational Materials Science*, Vol. 35, pp.432–441.

Maiti, A., Wescott, J. and Kung, P. (2005) 'Nanotube-polymer composites: insights from Flory-Huggins theory and mesoscale simulations', *Molecular Simulation*, Vol. 31, pp.143–149.

Marques, M.A.L., Troiani, H.E., Miki-Yoshida, M., Jose-Yacaman, M. and Rubio, A. (2004) 'On the breaking of carbon nanotubes under tension', *Nano Letters*, Vol. 4, pp.811–815.

Molinero, V. and Goddard, W.A. (2005) 'Microscopic mechanism of water diffusion in glucose glasses', *Physical Review Letters*, p.95.

Pharr, G.M., Oliver, W.C. and Brotzen, F.R. (1992) *Journal of Materials Research*, Vol. 7, No. 3, p.613.

Plimpton, S.J. (1995) 'Fast parallel algorithms for short-range molecular dynamics', *J. Comp Phys*, Vol. 117, pp.1–19.

Pugno, N.M. and Ruoff, R.S. (2004) 'Quantized fracture mechanics', *Philosophical Magazine*, Vol. 84, pp.2829–2845.

Qi, H.J., Teo, K.B.K., Lau, K.K.S., Boyce, M.C., Milne, W.I., Robertson, J. and Gleason, K.K. (2003) 'Determination of mechanical properties of carbon nanotubes and vertically aligned carbon nanotube forests using nanoindentation', *J. Mechanics and Physics of Solids*, Vol. 51, pp.2213–2237.

Ruan, C., Zeng, K. and Grimes, C.A. (2003) 'A mass-sensitive pH sensor based on a stimuli-responsive polymer', *Analytica Chimica Acta*, Vol. 497, No. 1, pp.123–131.

Shiratori, S.S. and Rubner, M.F. (2000) 'pH-dependent thickness behavior of sequentially adsorbed layers of weak polyelectrolytes', *Macromolecules*, Vol. 33, p.4213.

Sneddon, I.N. (1965), 'The relation between load and penetration in the axisymmetric boussinesq problem for a punch of arbitrary profile', *International Journal of Engineering Science*, Vol. 3, pp.47–57.

Tai. K., Dao, M., Suresh, S., Palazoglu, A. and Ortiz, C. (2007) 'Nanoscale heterogeneity promotes energy dissipation in bone', *Nature Materials*, Vol. 6, No. 6, pp.454–462.

Tai, K., Ulm, F.J. and Ortiz, C. (2006) 'Nanogranular origins of the strength of bone', *Nano Letters*, Vol. 6, No. 11, pp.2520–2525.

Underhill, P.T. and Doyle, P.S. (2004) 'On the coarse-graining of polymers into bead-spring chains', *Journal of Non-Newtonian Fluid Mechanics*, Vol. 122, pp.3–31.

Yeak, S.H., Ng, T.Y. and Liew, K.M. (2005) 'Multiscale modeling of carbon nanotubes under axial tension and compression', *Physical Review B*, Vol. 72.

Zhang, W.D., Yang, F. and Gu, P.Y. (2005) 'Carbon nanotubes grow to pillars', *Nanotechnology*, Vol. 16, pp.2442–2445.

Zhou, L.G. and Shi, S.Q. (2002) 'Molecular dynamic simulations on tensile mechanical properties of single-walled carbon nanotubes with and without hydrogen storage', *Computational Materials Science*, Vol. 23, pp.166–174.